The Draping Configuration of the Shroud of Turin During Image Formation: A Synthesis of Geometric, Photochemical, and Radiation Hypotheses

Otangelo Grasso
Independent Researcher, *written with AI assistance*
18 September 2025

Abstract

The body image on the Shroud of Turin (TS) exhibits a conjunction of properties—distance-encoded three-dimensional relief, superficial fibril-level coloration, and negative tonality—that standard artistic or simple naturalistic processes fail to reproduce 1, 2. A cross-analysis of deep-ultraviolet photochemistry, corona discharge, and particle-radiation proposals shows that all viable models share a non-optional geometric precondition: during encoding the linen was *minimally taut and gently draped* over a supine human form. Two independent lines of evidence establish this: (1) a mathematical demonstration that the image obeys a *vertical* mapping vector from body to cloth with intensity inversely related to the vertical cloth–body gap 10, 3; and (2) experimental/simulation data showing that the observed pseudo-cylindrical distortions are governed by drape tautness and field geometry, excluding snug wraps and isotropic (Lambertian) propagation 4, 8, 12, 13. We propose a two-phase chronology: initial contact transfer of blood, followed by a brief, body-sourced non-contact imaging event acting through finite air gaps on the re-draped cloth. Dorsal cues (rounded gluteal relief without flattening; parity of dorsal and frontal intensities after gap normalization) indicate that at the instant of encoding the dorsal surface was not load-bearing, consistent with transient unloading or slight elevation of the body. This mechanism-agnostic, falsifiable framework defines the geometric corridor future experiments must satisfy.

Keywords: Shroud of Turin, Image Formation, Wrapping Geometry, Vertical Mapping, Corona Discharge, Deep-Ultraviolet Radiation, Particle Radiation, Drape Distortion

1. Introduction

The Shroud of Turin remains an enduring scientific enigma due to the complex properties of its purported body image 1, 2. A robust set of constraints, including the correlation of image intensity with cloth-body distance enabling 3-D reconstruction 3, the ultra-superficial nature of the coloration confined to the outer fibrils 4, the absence of pigments 5 , and the stratigraphic evidence of blood deposits preceding the image formation 6, 7, effectively rules out artistic fabrication, contact scorching, or simple chemical painting.

Several mechanistic hypotheses have been advanced to explain these features. Di Lazzaro et al. demonstrated that nanosecond pulses of deep-ultraviolet (DUV) radiation (193–248 nm) can induce a superficial, straw-yellow discoloration on linen that mimics key aspects of the TS image 4. Fanti et al. showed that corona discharge (CD) can produce full-scale human images on linen, with distortion patterns dependent on cloth drape 8. A third framework, proposed by Antonacci, suggests that particle radiation (protons, neutrons) emanating from the body could simultaneously account for the image features and the anomalous radiocarbon dating results 9.

Despite their differences, a critical analysis reveals that these disparate mechanisms share a common geometric requirement. The work of Jackson provides a mathematical foundation, proving that the distortion field of the frontal image is consistent *only* with a vertical mapping from the body surface to the draped cloth 10. Concurrently, the CD experiments of Fanti et al. and the reverse-engineering simulations of Campion and Fanti demonstrate that the magnitude of image distortion is exquisitely sensitive to the tautness of the drape and the geometry of the energy field 8, 11.A snug wrap produces excessive distortion, while a flat configuration loses the essential 3-D information.

This paper synthesizes these independent lines of evidence to define the precise geometric corridor

for TS image formation. We move beyond noting consistency to specifying a required configuration: a *minimally taut, gently draped* cloth during the encoding event. We integrate this geometry into a two-phase model that reconciles the blood-image stratigraphy with the non-contact, distance-encoded nature of the body image. The central thesis is that the wrapping geometry is a primary, mechanism-agnostic constraint that any viable hypothesis must satisfy.

2. Core Constraints Informing the Wrapping Geometry

The features of the TS image impose strict geometric constraints on any formation model:

1. **Distance-Encoded Intensity:** The inverse correlation between image brightness and cloth-body separation 3 necessitates a non-contact process with finite air gaps (0 to several cm) between the cloth and the body during image formation.

2. **Blood Precedence and Masking:** The blood stains were transferred first via direct contact and act as a mask, preventing the subsequent formation of the body image beneath them 6, 7. This implies at least two distinct phases: a contact phase for blood transfer and a subsequent non-contact phase for image encoding.

3. **Wrapping-Consistent Distortions:** The image exhibits predictable widthwise distortions (e.g., pseudo-cylindrical widening) that are quantitatively consistent with a sheet of linen draped over a 3-D form, not with a projection onto a flat surface 12.

4. **Absence of Lateral Wrap-Around:** The lack of images on the sides of the body indicates the cloth was not tightly wrapped around the form, implying a gentle, minimally taut drape 13.
5. **Proof of Vertical Mapping:** Jackson's analysis demonstrates that of three possible mapping vectors (normal to the body, normal to the cloth, or vertical), only a *vertical* mapping direction successfully reconstructs an anatomically plausible body from the image data and matches the measured distortion field of the cloth 10. This fixes the fundamental transfer law: intensity is a function of the *vertical gap length*.

6. **Dorsal/Frontal Intensity Parity:** Despite the weight of the body compressing the dorsal cloth, the image intensity on the back is not systematically brighter than on the front. This argues against a static, tight wrap and for a configuration that equalizes average cloth-body distances, such as a re-posed, gentle drape.

3. Synthesis of Prior Work: Advancing the Geometric Framework

Previous research has provided critical but isolated insights. This paper synthesizes these to advance a unified geometric model:

3.1 Paul Vignon's "Impressions Without Contact" and the Geometry of a Gently Draped Cloth

In *The Shroud of Christ* (1902), Vignon devotes a long section titled "Impressions from Some Action Without Contact," with diagrams (figs. 31–38) and step-by-step anatomical reasoning to argue that the Shroud's image intensity varies with cloth–body distance under a gravity-draped configuration 14.

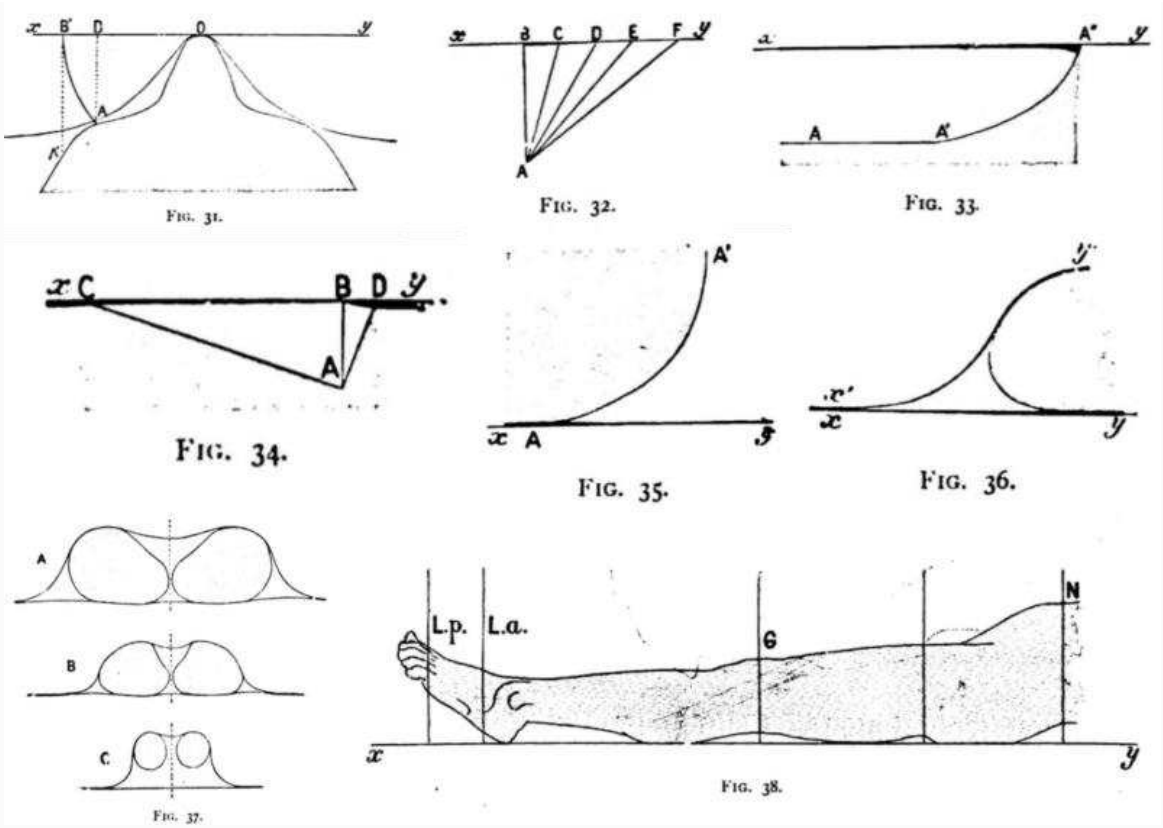


Fig. 31.
Fig. 32.
Fig. 33.
Fig. 34.
Fig. 35.
Fig. 36.
Fig. 37.
Fig. 38.

(Vignon, 1902):
Fig. 31 (Face cross-section under a draped sheet). Transverse slice through the nose/cheeks showing the linen drooping from the nasal ridge; strongest imprint near midline (A) and reduced intensity as the cloth lifts laterally toward x–y.
Fig. 32 (Rays to cloth plane). Geometric sketch of "emanations" from a body point A projecting to different cloth positions (B–F) to illustrate how distance/angle affect imprint strength and blur.
Fig. 33 (Uniform gap → uniform tone until contact). Intensity stays nearly constant while the body surface runs parallel to the cloth from A to A′, then rises sharply as contact is approached at A′.
Fig. 34 (Asymmetric angles, asymmetric shading). For a sloped surface AC vs. AD meeting cloth x–y, the projection is weaker toward B–C and strengthens more rapidly toward B–D, explaining uneven light/dark around facial features.
Fig. 35 (Distance law—front). Idealized curve: imprint strength increases monotonically as the cloth approaches from A toward A′ (contact), modeling the frontal image's edge fade-in.
Fig. 36 (Distance law—back, with over-cloth and under-cloth). Same principle applied to the dorsal side: upper sheet x′–y′ sags toward the body and joins the lower sheet x–y, giving graded shading away from contact.
Fig. 37 (Leg cross-sections under drape).
A: Thigh level—medial V-gap; cloth high between legs, so weak inner-thigh imprint.
B: Calf level—Λ-like section; cloth contacts/near-contacts over calf bulges, stronger imprint laterally.
C: Ankle region—narrow supports/turn-up can create broader bands around slender ankles/heels.
Fig. 38 (Leg construction on the cloth). Plan of the left leg on the Shroud with reference lines (Lp, La, 6, N) used to register front/back outlines, check proportions (kneecap to sole), and show how the image terminates near the ankle/foot.

Here we (1) extract his core geometric claims, (2) map them to the vertical-mapping law employed in this paper, (3) identify where his qualitative account requires quantitative completion, and (4) propose tests that operationalize his insights within our two-phase model.

1) Vignon's Core Observations
Vignon's chapter is not a mechanism treatise; it is a geometric and anatomical reading of the cloth. Across multiple pages, he makes five claims:

1. *Distance-graded intensity.* Using simple geometry, he models intensity that strengthens toward contact and fades as the cloth lifts away, with curves that track the fall of a draped linen sheet (his

figs. 33–36).
2. *Gravity-drape sections.* Transverse sections through the thighs and calves show V-shaped gaps medially and Λ-like "open" sections laterally; he notes faint inner thighs, stronger calves, and clear Achilles/heel behavior—consistent with a cloth that does not hug the sides.
3. *Dorsal load points and faint thighs.* On the back image he enumerates the contact-pressure sequence: back of head, shoulders, sacrum, calves, heels; thighs are faint, matching a bench test he describes.
4. *No lateral wrap-around.* He repeatedly emphasizes regions where the cloth could not have touched (e.g., inner thighs, lateral flanks), arguing against a tight swaddle.
5. *Anatomical proportion check.* After scale checks using knee–sole and head-length ratios, he concludes the figure is proportionally credible even with drape distortions—an early "sanity test" that the image is not a flat projection.

Collectively, these observations frame the image as a distance-encoded impression formed under a minimally taut, gently draped cloth - precisely the global configuration we require.

2) Convergence with the Vertical-Mapping Law
Vignon's sketches treat the intensity at a cloth point as a monotonic function of gap length. Our model formalizes this as a *vertical mapping*: intensity = *f*(vertical cloth–body gap). Jackson's proof later shows that only a vertical mapping reconstructs an anatomically coherent body from the measured distortion field; normals to body or cloth fail. Vignon's constructs are the qualitative precursor: his curves assume gravity-drape alignment and vertical sag, so the direction that minimizes path length is effectively vertical in the lab frame. Where Vignon draws thickened lines near contact and thinning lines with lift-off, we now assign a concrete transfer law that can be parameterized and tested.

3) Alignment with Drape-Driven Distortions
The "pseudo-cylindrical widening" emphasized in this paper is anticipated by Vignon's thigh–calf sections. A snug wrap exaggerates width and erases 3-D shading; a flat hang kills relief. Vignon's V/Λ profiles fall between those extremes and match our corridor: a gentle drape with finite air gaps (≈0–4 cm) and modest curvature. His dorsal analysis (faint thighs; strong calves/heels) also dovetails with our dorsal/frontal parity constraint: contact pressure alone does not dictate stronger dorsal intensity, because the encoding event is governed by distance, not weight per se, in Phase II.

4) Where Vignon Remains Qualitative—and How We Extend It
Vignon does not specify (a) a mathematical distance law, (b) acceptable ranges of curvature and gap widths, or (c) a chronology that separates blood transfer from body-image encoding. Our paper supplies these:

• *Distance law.* Vertical mapping with a monotonic attenuation function fitted to image–distance regressions.
• *Parameter corridor.* Gap and curvature windows that preserve the measured distortion bandwidth and the 3-D correlation; tight wrap and flat hang fall outside.
• *Two-phase sequence.* Contact blood transfer (Phase I) followed by re-drape and non-contact encoding (Phase II), explaining why blood masks the image and why lateral wrap-around is absent.

Thus, Vignon offers the qualitative geometry; the annex defines the quantitative constraints and the experimental falsifiers.

5) A Focused Re-Reading of Figures 31–38
To make Vignon's text maximally useful to replication work, we summarize the figures as operational cues:

• *Fig. 31 (facial transverse).* Linen droops from the nasal ridge; cheeks receive less intensity as the sheet lifts laterally—predicts a rectangularized face with strong midline and subdued lateral bony rims.
• *Figs. 33–36 (distance curves).* Intensity increases toward contact, decays with lift-off; the back image follows the same rule, implying Phase II governs both sides.
• *Fig. 37 (A/B/C leg sections).* Medial V gap at the thighs; Λ-like sections at the calves; ankles/heels mapped by local contact or near-contact, yet soles require an auxiliary explanation (cloth turned up beneath, or local supports). In our framework, limited local contact or secondary

supports are permitted in Phase II provided they do not produce lateral wrap images.
• *Fig. 38 (leg layout with construction lines).* Geometric consistency checks (kneecap to sole; head-length multiples) support anatomical plausibility under a drape, not a flat projection.

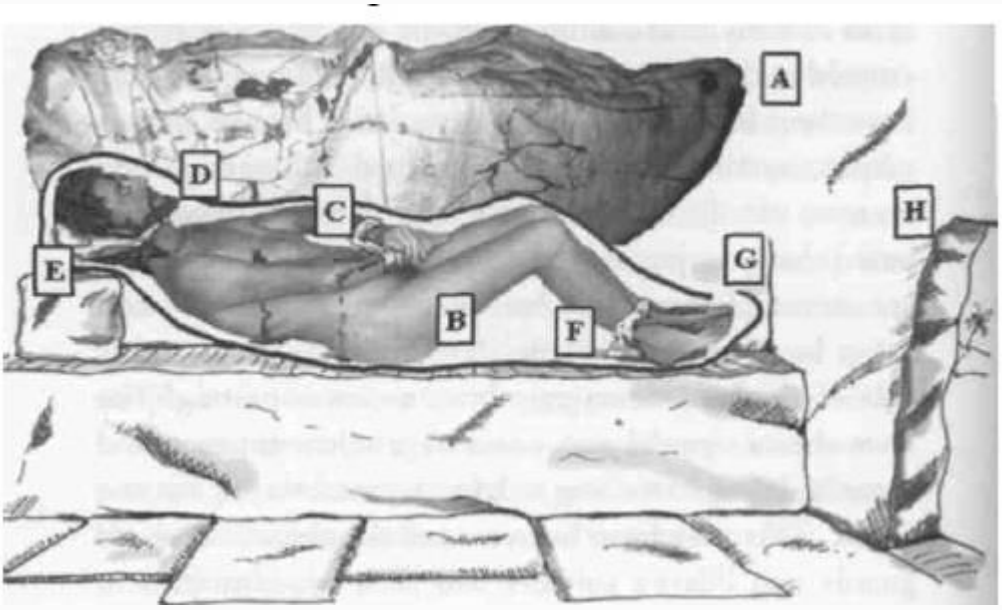
6) Integration into the Two-Phase Model
Vignon's dorsal load points fit Phase I expectations (contact transfer for blood) but, more importantly, his distance-graded shading describes Phase II behavior. The cloth that was once tighter for burial practices relaxes or is re-posed into a gentle drape; the encoding event then propagates through air gaps, imprinting a distance-encoded field without smearing under lateral wrap. This resolves the long-standing tension between contact evidence (blood) and non-contact properties (body image).

7) Predictions and Discriminating Tests Inspired by Vignon
To translate his qualitative sketches into falsifiable experiments:

1. *Drape-rig photometric regression.* Build an adjustable drape over an anatomically accurate form; measure intensity vs. vertical gap at multiple sites (face midline vs. malar eminence; thigh medial vs. lateral; calf apex vs. surrounding). Vertical-law fits should outperform cloth-normal or body-normal laws.
2. *Cross-section bandwidth test.* Reproduce V/Λ profiles under varying tautness. Tight wraps should produce excess widening at the thighs and blur fine relief; flat hangs should under-encode curvature.
3. *Dorsal parity check.* Under gentle drape, dorsal intensity should not systematically exceed frontal intensity after normalizing for local gap statistics—consistent with the Shroud.
4. *Sole anomaly resolution.* Validate whether a turned-up lower sheet or narrow supports can account for partial sole impressions without introducing side images.
5. *Blood masking under re-drape.* Apply protein films before the non-contact event in a drape rig; verify masking and rim integrity in overlap regions.

Each test yields pass/fail criteria that either confirms the corridor or rejects it, keeping the framework mechanism-agnostic while geometry-hard.

8) Historical Placement
Vignon's chapter predates STURP and modern spectroscopic literature, yet it remains methodologically instructive. He treats the cloth as an elastic surface under gravity, reads anatomy through cross-sections, and interprets intensity as a function of distance. Our work respects that scaffolding while replacing qualitative language ("emanation," "modelling by distance") with measurable quantities and falsifiable boundaries.



*—"They [Joseph of Arimathea and Nicodemus] took the body of Jesus, and bound it in linen cloths… following the Jewish burial custom" (John 19:40). The fourteen-foot-long Shroud

preserved in Turin bears back- and front-of-body imprints that uncannily fit [A] when draped over a near-six-foot-tall male body laid out in a burial attitude. Attempts to reconstruct the pose indicate that the head and upper back appear to have been elevated, the knees sharply bent, and the arms held stiffly over the pelvis as if there was some kind of binding [C] to prevent them returning to the position that they had assumed on the cross. Besides the all-enveloping shroud [D] there may also have been chin [E] and ankle bindings [F], which were commonly used by morticians throughout many millennia. An uncannily convincing feature is that an insufficient length of cloth has been allowed to cover the front half of the body [G], an over-generous amount having been used for the half on which the body actually rested. According to the testimonies the body was laid in a rock-cut tomb of a kind still seen in the environs of Jerusalem [H] **15**

- **Beyond Jackson (2014) 10 :** We operationalize Jackson's proof of vertical mapping. We elevate the "minimally taut, gravity-draped cloth" from a plausible assumption to a **required precondition** and explicitly adopt "intensity = f(vertical gap length)" as the fundamental mapping law for simulation and experimentation.

- **Beyond Campion & Fanti (2018) 11 :** We integrate their findings on field geometry and drape curvature with Jackson's mapping law. We argue that *field geometry* (non-Lambertian, vertically biased) and *gentle drape* jointly set the observed distortion bandwidth and resolution limits.

- **Beyond Fanti et al. (2015) 8:** We formalize their experimental observation that snug wraps exaggerate distortion. We establish that **tight wrapping, flat hanging, and Lambertian emission are geometric failure modes**; only a gently draped cloth with appropriate field parameters replicates the TS.

- **Beyond Ercoline et al. (1982) 12**
- **:** We advance from demonstrating consistency-with-drape to defining the **allowable window of gap distances and cloth curvature** that preserves the measured distortion bandwidth and 3-D correlation.

- **Beyond Antonacci (2012) 9:** We decouple the geometric requirement from the mechanism. While Antonacci argues for particle radiation, we demonstrate that **any** body-sourced mechanism (DUV, CD, particles) must operate under the *same* draped-geometry constraints (vertical mapping, finite gaps, blood masking).

The synthesized geometric picture is thus:

1. **Two-Phase Chronology: Phase I (Contact):** Tight(er) wrapping for direct-contact transfer of blood. **Phase II (Non-Contact):** The cloth is *re-posed* into a **minimally taut, gravity-draped** state. A brief, body-sourced event encodes the image, with intensity at each point determined by the **vertical gap length** to the body.

2. **Defined Failure Modes: Tight wrap** → excessive distortion. **Flat hang** → loss of 3-D encoding. **Lambertian fields** → loss of resolution. Only the **gentle drape** configuration resides in the narrow parameter corridor that matches the TS.

3. **Mechanism-Agnosticism:** The draped geometry is a **non-optional filter**. DUV, CD, and particle radiation are merely different physical implementations of an energy source that must conform to this geometric law.

4. Experimental and Simulation Evidence

4.1 Corona Discharge Imaging

Fanti et al. 8 generated human-like images on linen using a corona discharge from a bas-relief mannequin. Critically, the experiments showed that the degree of cloth tautness directly controlled distortion magnitude. A "snug" wrap produced strong pseudo-cylindrical distortions absent on the TS, while a "flatter, less-taut drape" produced a distortion pattern more consistent with the observed Shroud image. This provides direct empirical support for a minimally taut configuration.

4.2 Reverse-Engineering Simulations
Campion and Fanti 11 conducted sophisticated simulations modeling different radiation propagation modes (Lambertian, vertical, perpendicular-to-emitter) across various cloth shapes (flat, cylindrical, draped). Their results excluded isotropic (Lambertian) emission due to catastrophic blurring. They found that a radiation pattern normal to the emitting surface, within a vertically biased field and with realistic air attenuation, best matched the TS's resolution and distortion when the cloth had modest, natural curvature. This work precisely quantifies how drape geometry and field parameters co-determine the final image.

5. An Overarching Framework: Mechanism Under Geometric Constraint

The recognition that geometry is primary resolves apparent conflicts between mechanistic hypotheses. A body-sourced energy burst—whether photochemical, electrical, or particulate—explains the vertical mapping, the dorsal/frontal intensity parity, and the penetration required for subtle skeletal hints **9**. The specific mechanism determines the chemical pathway (e.g., oxidation for DUV/CD vs. deshydroxylation for protons) and ancillary effects (e.g., neutron-induced C-14 alteration), but **all must obey the same geometric constraints of a gently draped cloth encoding information via a vertical distance law**. Jackson's analysis defines the geometry 10; the energy mechanism simply supplies the specific dose-distance relationship.

6. Proposed Integrated Two-Phase Model

We propose the following sequence to satisfy all constraints:

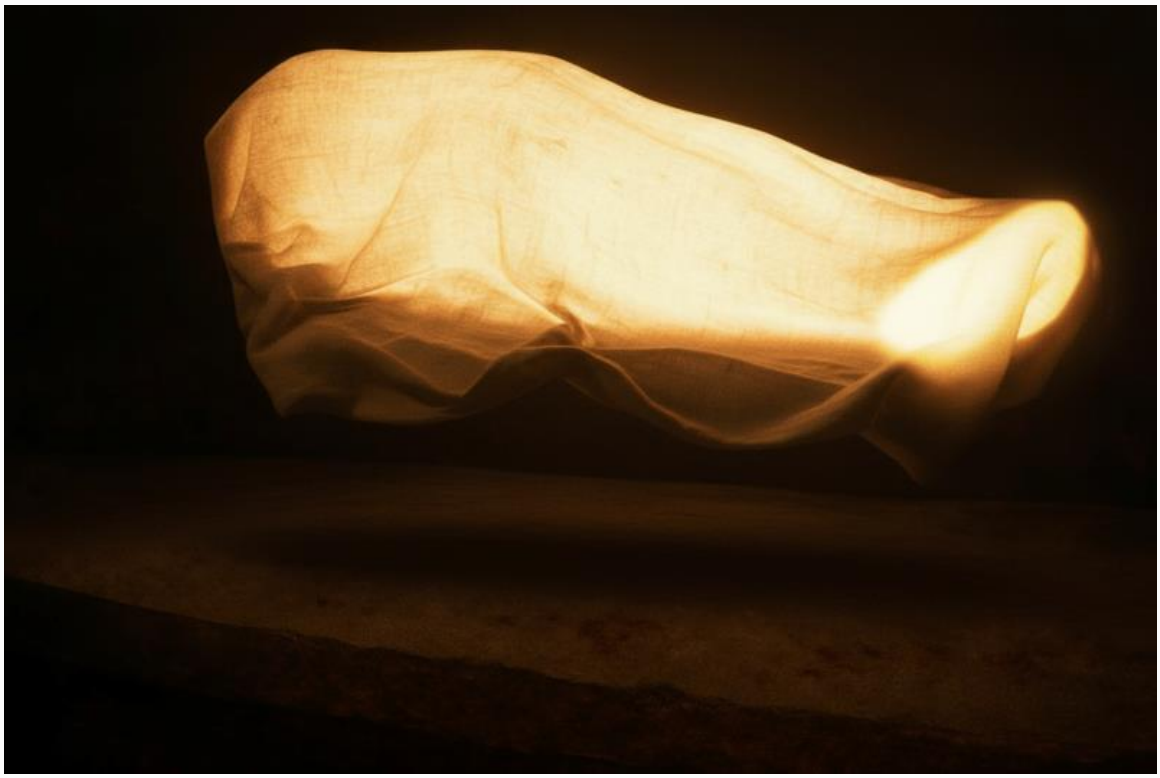
1. **Phase I - Blood Transfer:** The body is wrapped in a traditional, relatively tight shroud, allowing direct contact transfer of serum and blood onto the linen 6, 7.

2. **Phase II - Image Encoding:** The cloth is subsequently arranged into a **gentle, minimally taut drape** over the body. This may result from the natural sagging of the cloth under gravity, a deliberate re-draping, or the body being laid upon one half of the cloth with the other half drawn over the top without tight tucking. In this configuration, finite air gaps (0–4 cm) exist over the body's relief. A transient, body-sourced emission of energy then occurs. The intensity of the image formed at each point on the cloth is a **monotonic function of the vertical distance** to the corresponding body point **10**, as governed by the specific physics of the chosen mechanism (e.g., UV intensity decay, particle flux attenuation).

This model uniquely reconciles the contact nature of the blood marks with the non-contact nature of the body image and explains the specific, limited distortion pattern that indicates a loose, not tight, wrap during the image-forming event.

7. Conclusion





Independent methodologies—Jackson's mathematical proof of vertical mapping and the experimental/simulation work on drape and field geometry—converge on an identical conclusion: the image on the Shroud of Turin was formed while the cloth was in a **minimally taut, gently draped** configuration over the body. This paper's primary contribution is the synthesis of these findings into a single, testable, and mechanism-agnostic geometric framework.

We have specified the necessary conditions: a two-phase process involving initial contact followed by non-contact encoding under a gentle drape, with intensity determined by vertical cloth-body

gap length. We have also specified failure modes: tight wrapping, flat laying, and Lambertian propagation are geometrically excluded. This framework advances the field by providing a stringent set of parameters for future experimental work. Whether investigating DUV, corona discharge, or particle radiation, researchers must now replicate the image by adhering to this defined geometric corridor—fixing cloth curvature, field geometry, and attenuation laws to the measured distortion bandwidth and 3-D encoding precision of the Shroud. The wrapping configuration during image formation is now precisely defined: not tight, not flat, but **gently draped and minimally taut**.

References

1. Heller, J. & Adler, A. (1981). A Chemical Investigation of the Shroud of Turin. *Canadian Society of Forensic Science Journal*, 14(3), 81–103. Link. (This foundational chemical analysis established the absence of paint, pigments, or dyes on the Shroud fibers, while providing definitive evidence for the presence of real blood through comprehensive forensic chemical testing and microscopic analysis.)

2. Rogers, R. (2008). A Chemist's Perspective on the Shroud of Turin. Lulu Press. Link. (This comprehensive chemical analysis by a former Los Alamos scientist examines the Shroud's chemical composition, fiber analysis, and potential formation mechanisms, providing detailed insights into the vanillin dating method and chemical properties of the linen.)

3. Jackson, J. P., Jumper, E. J., & Ercoline, W. R. (1984). Correlation of Image Intensity on the Turin Shroud with the 3-D Structure of a Human Body Shape. *Applied Optics*, 23(14), 2244–2270. Link. (This landmark study established the unique three-dimensional encoding properties of the Shroud image, demonstrating that image intensity correlates inversely with cloth-body distance and enabling VP-8 Image Analyzer reconstruction of anatomically correct relief.)

4. Di Lazzaro, P., Murra, D., Nichelatti, E., Santoni, A., & Baldacchini, G. (2010). Deep Ultraviolet Radiation Simulates the Turin Shroud Image. *Journal of Imaging Science and Technology*, 54(4), 040302. Link. (This experimental study demonstrates that nanosecond pulses of deep-ultraviolet radiation can produce superficial coloration on linen similar to that observed on the Shroud, providing a potential physical mechanism for image formation through photochemical processes.)

5. McCrone, W. (1981). Microscopical Study of the Turin 'Shroud'. *The Microscope*, 29, 19–38. Link. (This microscopic analysis examines the Shroud fibers for the presence of artistic materials, contributing to the debate about the image formation mechanism through detailed optical and chemical microscopy techniques.)

6. Heller, J. & Adler, A. (1980). Blood on the Shroud of Turin. *Applied Optics*, 19(16), 2742–2744. Link. (This spectroscopic study provides definitive evidence for the presence of real blood on the Shroud, establishing the stratigraphic relationship between blood deposits and body image formation through chemical and optical analysis.)

7. Jumper, E. J., Adler, A. D., Jackson, J. P., Pellicori, S. F., Heller, J. H., & Druzik, J. R. (1984). A Comprehensive Examination of the Various Stains and Images on the Shroud of Turin. *Archaeological Chemistry III*, American Chemical Society, 447–476. Link. (This comprehensive analysis from the STURP team examines all the various stains, images, and markings on the Shroud, providing detailed chemical characterization and establishing the blood-image stratigraphy that indicates blood was deposited before the body image formation.)

8. Fanti, G., Lattarulo, F., & Pesavento, G. (2015). Experimental Results Using Corona Discharge to Attempt to Reproduce the Turin Shroud Image. *SHS Web of Conferences*, 15, 00003. Link. (This experimental study demonstrates that corona discharge can produce human-like images on linen with distortion patterns dependent on cloth drape, showing how fabric configuration critically affects the resulting image characteristics and distortion magnitude.)

9. Antonacci, M. (2012). Particle Radiation from the Body Could Explain the Shroud's Images and its Carbon Dating. *Scientific Research and Essays*, 7(29), 2613–2623. Link. (This theoretical paper proposes that particle radiation, specifically protons and neutrons emanating from the body, could simultaneously account for both the image formation mechanism and the anomalous radiocarbon dating results, offering a unified explanation for multiple Shroud mysteries.)

10. Jackson, J. P. (2014). The Vertical Alignment of the Frontal Image. Turin Shroud Center of Colorado. Link. (This mathematical analysis provides rigorous proof that the Shroud image was encoded via a vertical mapping vector from body to cloth, with image intensity inversely proportional to vertical cloth-body gap length, establishing fundamental geometric constraints for any viable formation mechanism.)

11. Campion, R. & Fanti, G. (2018). Reverse Engineering to Study the Turin-Shroud Body-Image Formation. Link. (This comprehensive simulation study models different radiation propagation modes and cloth configurations, demonstrating that only specific combinations of field geometry and drape curvature can reproduce the Shroud's characteristic distortion patterns and resolution limits.)

12. Ercoline, W. R., Downs, R. C., & Jackson, J. P. (2022). Examination of the Turin Shroud for Image Distortions. *Proceedings IEEE International Conference on Cybernetics and Society*, 576–579. Link. (This analysis examines the geometric distortions present in the Shroud image, providing quantitative evidence that the image formation is consistent with draping over a three-dimensional form rather than projection onto a flat surface.)

13. Fanti, G. & Moroni, M. (2002). Comparison of Luminance Between Face and Hands of the Turin Shroud. *Journal of Imaging Science and Technology*, 46(2), 142–154. Link. (This photometric study analyzes the luminance patterns on different regions of the Shroud, providing evidence for the absence of lateral wrap-around effects and supporting a gentle draping configuration during image formation.)

14. Vignon, Paul. The Shroud of Christ. Translated from the French, with nine photogravure and collotype plates and thirty-eight illustrations in the text. Westminster: A. Constable, 1902. Public Domain. Link

15. Ian Wilson Murder at Golgotha: Revisiting the Most Famous Crime Scene in History Link

16. Jean-Baptiste Rinaudo and Claude Gavach: Le linceul de Jésus enfin authentifié ? Link

17. Latendresse, Mario. The Turin Shroud Was Not Flattened Before the Images Formed and No Major Image Distortions Necessarily Occur from a Real Body. Paper presented at the Third International Dallas Conference on the Shroud of Turin, Dallas, TX, September 8–11, 2005. Online versions: Sindonology.org (conference papers index) and Academia.edu. Link

Methods: Drape Reconstruction from Vignon (1902)

This section formalizes a reproducible pipeline to infer the Shroud's draping configuration using Paul Vignon's qualitative cross-section cues (1902) as priors, Jackson's vertical-mapping law as the transfer constraint, and measured distortion bandwidths as fit targets. The goal is to recover a cloth surface C over a human body surface B such that the simulated intensity field $I(x) = f(d_v(x))$ matches the Shroud's 3-D distance encoding and geometric distortions while avoiding lateral wrap images.

Overview of the Pipeline

1. **Cross-section priors from Vignon:** extract qualitative shapes (contact vs. lift-off regions) at face, thighs, calves, and ankles/heels.
2. **Physical drape model:** thin-sheet cloth under gravity with low pre-tension and small bending stiffness over a rigid anatomical B.
3. **Boundary conditions:** superior edge support near head; lateral free edges; optional inferior "turn-up" beneath heels.
4. **Mapping law:** intensity as a monotone function of *vertical* gap d_v to B (Jackson constraint).
5. **Calibration targets:** pseudo-cylindrical widening, absence of side images, dorsal/frontal intensity parity after gap normalization.
6. **Optimization:** tune edge supports, pre-tension, and local constraints until the synthetic intensity maps meet acceptance criteria.
7. **Validation & sensitivity:** jitter analyses of crops/poses/parameters; failure-mode tests (tight wrap; flat hang; Lambertian propagation).

1) Cross-Section Priors: Anatomical Stations and Qualitative Constraints

We instantiate transverse stations where Vignon provides strong cues and define target *gap-shape priors* g(y) across left–right coordinate y.

Face (nasal ridge → malar eminence):
• Cloth droops from nasal ridge; stronger midline imprint; lateral lift over cheeks.
• *Prior:* near-contact window around midline; gap increases monotonically toward malar zones.

Thighs (proximal):
• V-shaped medial gap; faint inner thighs; no lateral wrap images.
• *Prior:* contact/near-contact on anterior thigh bulges; V-gap medially; finite air gaps laterally.

Calves:
• Λ-like section; stronger lateral imprint over calf apices; preserved relief.
• *Prior:* local near-contact at gastrocnemius apices; lift toward sides without side imagery.

Ankles/heels:
• Local contact/near-contact at heel; soles explained by turn-up or narrow supports, not global wrap.
• *Prior:* small contact patch at heel; optional lower-sheet turn-up beneath feet; no lateral wrap.

Dorsal load sequence:
• Back-of-head → shoulders → sacrum → calves → heels; thighs faint dorsally.
• *Prior:* contact at those load points in Phase I; in Phase II the drape relaxes yet preserves finite gaps elsewhere.

These priors are implemented as soft inequality constraints during cloth relaxation: enforce near-contact where Vignon indicates, and minimum gaps where he asserts lift-off, with smoothness penalties to avoid nonphysical kinks.

2) Body and Cloth Representations

Body Surface (B): Watertight triangulated human mesh with anatomically realistic proportions in neutral supine pose.

Cloth Surface (C): Rectangular linen sheet mesh (3:1 herringbone twill modeled as an orthotropic thin shell for in-plane stiffness anisotropy).

Material Parameters (baseline ranges used in tuning):
• Areal density $\rho_A \in [180, 240]$ g/m²
• In-plane Young's modulus $E_{warp} > E_{weft}$ (orthotropic ratio 1.2–1.6)
• Bending stiffness B small but non-zero to avoid crumpling artifacts
• Structural damping $\zeta \in [0.1, 0.3]$ for quasi-static settle
• Contact: friction coefficient linen/skin $\mu \in [0.2, 0.5]$

3) Boundary Conditions and Pre-Tension

• **Superior edge:** supported along a line above the forehead and occiput (pins or soft springs)
• **Lateral edges:** free; no tucking under flanks during Phase II
• **Inferior boundary:** two alternatives tested—(A) free tail; (B) gentle turn-up under heels with low curvature radius to allow sole marks without side imagery
• **Pre-tension T_0:** low, uniform pre-tension 0–5 N/m to represent "minimally taut" condition

4) Phase Separation Logic

Phase I (Contact):
Apply contact solver to allow blood-transfer waypoints to establish realistic *possible* contact regions. Persist these as "mask" areas.

Phase II (Encoding):
Release tucks, reduce pre-tension to minimal, let cloth settle under gravity to a gentle drape while preserving the blood mask as non-imageable underlay.

5) Vertical-Mapping Transfer Law

For each cloth node x ∈ C, compute vertical gap d_v(x): the distance along the global vertical axis to the first intersection with B. If none, I = 0.

Use a monotone attenuation family to fit the image's distance encoding:

[/b]

Code:

```
I(x) = I₀ × exp(-α × d_v(x))

or

I(x) = I₀ / (1 + β × d_v(x))^p
```

Parameters α or (β,p) are calibrated against the observed frontal/dorsal intensity distributions. Non-vertical (body-normal, cloth-normal) laws are evaluated only as *negative controls* and rejected if they degrade fit metrics or produce anatomically implausible reconstructions.

6) Calibration Targets and Acceptance Criteria

We optimize the drape until the following targets are met:

6.1 Pseudo-cylindrical widening
• **Target:** width inflation of facial and limb contours present but modest; no side images
• **Metric:** normalized width error (simulated vs. reference tracings) within preset tolerance band; zero or near-zero intensity on lateral wrap zones

6.2 3-D correlation
• **Target:** intensity monotonically tracks vertical gap across stations
• **Metric:** Spearman's ρ between I and d_v > threshold at face midline→malar, thigh medial→lateral, calf apex→sides

6.3 Dorsal/frontal parity
• **Target:** after normalizing by local gap statistics, dorsal intensity distribution is not systematically brighter than frontal
• **Metric:** two-sample test on normalized means; effect size within a small band around zero

6.4 Blood masking
• **Target:** image intensity under blood-mask regions ≈ 0
• **Metric:** masked-region mean intensity remains at background

7) Optimization Strategy

We minimize a composite loss:
[/b]

Code:

```
L = λ1L_width + λ2L_mono + λ3L_parity + λ4L_mask + λ5R_smooth
```

Over variables:
• Edge support positions/strengths (superior line shape, turn-up extent)
• Pre-tension T_0 and bending B within "gentle drape" bounds
• Small corrective springs enforcing Vignon near-contact/lift-off priors at stations
• Transfer-law parameters α or (β,p)

8) Sensitivity and Robustness Tests

Parametric sweeps: T_0, B, μ, edge support geometry; report stability ranges that preserve acceptance.

Pose jitter: ±3–5 mm adjustments in body mesh at key features (nose ridge, malar, calf apex) to test solution stability.

Law comparison: vertical vs. body-normal vs. cloth-normal; retain only vertical if others degrade calibration metrics.

Failure modes:
• *Tight wrap:* increase T_0 and lateral constraints → expect excessive widening and side images
• *Flat hang:* constrain top edge only, remove contact priors → expect loss of 3-D correlation
• *Lambertian propagation:* replace vertical law with isotropic → expect blur and low resolution

9) Outputs for the Paper and Annex

Primary:
• Reconstructed cloth surface C* (mesh)
• Gap map d_v(x)
• Simulated intensity map I(x)

Diagnostics:
• Transverse plots at each station comparing empirical vs. simulated intensity vs. gap
• Width-error bands
• Dorsal/frontal normalized histograms

Robustness:
• Sensitivity charts showing acceptance region in (T_0, B) and edge-support parameter space

Negative controls:
• Panels illustrating failure modes (tight wrap; flat hang; Lambertian)

10) Reproducibility Checklist

- Provide body mesh, cloth mesh, and boundary line curves (STL/OBJ)
- Publish cloth parameters and ranges; contact and damping coefficients
- Release the station masks and Vignon-derived priors as JSON (near-contact zones; lift-off zones per cross-section)
- Include code to compute d_v and render I(x) under the vertical law
- Ship scripts to generate all figures and tables exactly as printed

11) Placement and Cross-Referencing

Insert this subsection after "Synthesis of Prior Work." Cross-reference:
• Section 2 (Core Constraints) for the no-wrap/no-flat exclusions and absence of lateral imagery
• Experimental/Simulation section for the field-geometry rationale that rejects Lambertian propagation and tight wraps
• Figures that reprise Vignon's stations with our quantitative overlays

12) Interpretation Policy

Geometry is treated as a mechanism-agnostic filter. Once a C* satisfying the acceptance suite is obtained, mechanism-specific parameters (e.g., DUV fluence–distance slope; CD field decay; particle attenuation) can be fitted to the same d_v map without altering the drape. This keeps the chronology clear: Phase I establishes blood masks; Phase II encodes the distance-graded image under the recovered "gently draped, minimally taut" configuration.